FINITE ELEMENT MODELING OF ULTRASPORT HELICOPTER CABIN

J. Oh, W. Liang and **A. Baz**

Mechanical Engineering Department
University of Maryland
College Park, MD 20742

ABSTRACT

The structural vibration of the cabin of Utrasport helicopter ATI-496 are studied. The dynamic behavior of the cabin is predicted by a Finite Element Model developed using 6-node elements, for simulated according to Kirchoff theory for plates. The natural frequencies of vibration and corresponding mode shapes of the cabin and its door are measured experimentally and used to validate the Finite Element model. The close agreement between experimental results and numerical predictions. The numerical and experimental validations demonstrate the accuracy of the developed model and emphasize its potential extension to investigate the application of smart materials for active control of vibration and noise radiation from hulls of aircrafts.

REPORT DOCUMENTATION PAGE

Form Approved
OMB NO. 0704-0188

1. AGENCY USE ONLY (Leave Blank)	2. REPORT DATE 6/2/00	3. REPORT TYPE AND DATES COVERED FINAL Report - 3/16/98-3/15/99

4. TITLE AND SUBTITLE
Vibration & Noise Monitoring of Large Observation Platforms

5. FUNDING NUMBERS
DAAG55-98-1-0206

6. AUTHOR(S)
Amr M. Baz

7. PERFORMING ORGANIZATION NAME(S) AND ADDRESS(ES)
University of Maryland
Mehanical Eng. Dept.
College Park, MD 20742

8. PERFORMING ORGANIZATION REPORT NUMBER

9. SPONSORING / MONITORING AGENCY NAME(S) AND ADDRESS(ES)
U. S. Army Research Office
P.O. Box 12211
Research Triangle Park, NC 27709-2211

10. SPONSORING / MONITORING AGENCY REPORT NUMBER
ARO 38784.1-EG-RIP

11. SUPPLEMENTARY NOTES
The views, opinions and/or findings contained in this report are those of the author(s) and should not be construed as an official Department of the Army position, policy or decision, unless so designated by other documentation.

12 a. DISTRIBUTION / AVAILABILITY STATEMENT
Approved for public release; distribution unlimited.

12 b. DISTRIBUTION CODE

13. ABSTRACT (Maximum 200 words)

Instrumentation is needed to monitor the vibration and noise of large platforms in order to evaluate the effectiveness of their operation as quiet and stable platforms for observation, target recognition and precision pointing. The evaluation process will involve the comprehensive monitoring of the vibration and noise fields of the platforms using multi-channel real-time data acquisition , analysis and recording system to be acquired through this DURIP program. With such monitoring capabilities, the mechanical and acoustic signatures of these platforms can be accurately determined, the sources of vibration and noise can be identified and appropriate control measures can be taken to minimize their interference with the successful operation of the platforms.

The proposed instrumentation will provide also a general purpose facility for on-ground and in-flight monitoring of critical systems such as the Viewing Imager/Gimballed Instrumentation Laboratory (VIGIL) of the Ballistic Missile Defense Organization (BMDO). Such thorough on-ground and during-flight testing is essential to ensuring satisfactory performance of these critical observation, target recognition and precision pointing platforms when deployed in space for autonomous operation.

14. SUBJECT TERMS Vibration & Noise Monitoring, Helicopter Cabin, Interior Noise	15. NUMBER OF PAGES 27
	16. PRICE CODE

17. SECURITY CLASSIFICATION OR REPORT	18. SECURITY CLASSIFICATION ON THIS PAGE	19. SECURITY CLASSIFICATION OF ABSTRACT	20. LIMITATION OF ABSTRACT
UNCLASSIFIED	UNCLASSIFIED	UNCLASSIFIED	UL

1. INTRODUCTION

Helicopters are susceptible to high levels of vibration and noise due to the unsteady aerodynamic environment in which the blades operate as well as the coupled structural mechanical system comprised of the rotor, fuselage, transmission and engine. The structure-borne vibration and noise isolation have been studied, for example, by Unruh [1, 2], Swanson et al. [3] and Sutton et al. [4], as means for reduced structure-borne noise transmission using engine isolator.

In this work, a finite element model is developed to predict the vibration and mode shapes of a helicopter cabin.

The model predictions are validated experimentally by measuring the mode shapes and natural frequencies of a full-size helicopter cabin and its door. The cabin is placed in an anechoic chamber and its vibration is measured by a scanning head laser vibrometer. Particular emphasis is placed in measuring the vibration of the door, in order to accurately predict its mode shapes and therefore study the optimal placement of actuators to reduce its vibration and the noise radiation inside the cabin. The structure is modeled using 3-node plate elements formulated according to Kirchhoff plate theory. The complete description of the element can be found in Bathe [5] and Razzaque [6]. The close agreement between the theoretical predictions and experimental data demonstrate the accuracy of the developed model.

The model can be extended to include the application of smart materials to actively control the vibration and the noise radiation from the structure inside the cabin.

The paper is organized in 4 sections and one appendix. In section 1, a brief introduction is given. The finite element model of the helicopter cabin is introduced in section 2. The experimental validation of the model predictions and the performance characteristics of the door and helicopter cabin are described in section 3. Section 4 summarizes the main results of this work and gives some recommendations for future research.

2. FINITE ELEMENT MODELING

A finite Element model is developed to describe the dynamic behavior of the Helicopter. The considered Shell element has both bending and membrane capabilities which permit both in-plane and normal loads. The element has six degrees of freedom at each node: translations in the nodal x, y, and z directions and rotations about the nodal x, y, and z axes. Stress stiffening and large deflection capabilities are included. A consistent tangent stiffness matrix option is available for use in large deflection (finite rotation) analyses. The geometry, node locations, and the coordinate system for this element are shown in Figure 1. The element is defined by three nodes, three thicknesses, an elastic foundation stiffness, and three orthotropic material properties. Orthotropic material directions correspond to the element coordinate directions. The element coordinate system orientation is described in Figure 1. The element coordinate system is used for orthotropic material input directions, applied pressure directions, and, under some circumstances, stress output directions.

The element coordinate systems are right-handed, orthogonal systems.

2.1 *Discrete Kirchhoff theory elements*

The formulation of the element is based on the discrete Kirchhoff theory for bending of thin plates. The element governing relations are obtained by including transverse shear deformations. In this case the independent quantities are the deflection w, and the rotations β_x and β_y, that need to satisfy continuity requirements. The transverse shear energy is neglected altogether and the Kirchhoff hypothesis is introduced in a discrete way along the edges of the element to relate the rotations to the transverse displacements.

The discrete Kirchhoff theory elements with transverse shear deformations uses a generalization of the Kirchhoff hypothesis: points of the plate originally on the normal to the undeformed middle surface remain on a straight line but which is not necessarily normal to the deformed middle surface. With this assumption the displacements of a point of coordinates x, y, z are:

$$\begin{aligned} u &= z\beta_x(x,y), \\ v &= z\beta_y(x,y), \\ \text{and} \quad w &= w(x,y) \end{aligned} \tag{1}$$

where w is the transversal displacement, β_x and β_y are the rotations of the normal to the undeformed middle surface in the x-z and y-z planes, respectively.

The linear strain expressions include the bending and transverse strains as follows:

$$\varepsilon_b = z\kappa \tag{2}$$

and

$$\gamma = \begin{bmatrix} w_{,x} + \beta_x \\ w_{,y} + \beta_y \end{bmatrix} \tag{3}$$

being ε_b and γ the bending and transverse strains. In equation (2) κ is the three component vector of curvatures:

$$\kappa = \begin{bmatrix} \beta_{x,x} \\ \beta_{y,y} \\ \beta_{x,y} + \beta_{y,x} \end{bmatrix} \tag{4}$$

The strain-stress relations are:

$$\sigma_b = \begin{bmatrix} \sigma_x \\ \sigma_y \\ \tau_{xy} \end{bmatrix} = z \begin{bmatrix} D_{11} & D_{12} & D_{13} \\ & D_{22} & D_{23} \\ & & D_{33} \end{bmatrix}, \ \kappa = z\mathbf{D}\kappa \tag{5}$$

and

$$\sigma_s = \begin{bmatrix} \tau_{xz} \\ \tau_{yz} \end{bmatrix} = \begin{bmatrix} E_{13} & E_{23} \\ E_{23} & E_{33} \end{bmatrix}, \ \gamma = \mathbf{E}\gamma \tag{6}$$

where $E_{i,j}$, $i, j = 1, 3$, are the components of the three-dimensional elasticity matrix and

$$D_{ij} = E_{ij} - \frac{E_{i3}E_{3j}}{E_{33}}.$$

With the kinematics as given by equations (1) through (4) and the material description as given by equations (5) and (6) the strain energy is:

$$U = U_b + U_s \tag{7}$$

where

$$U_b = \frac{1}{2}\int_A \kappa^T D_b \kappa \, dxdy \tag{8}$$

$$U_s = \frac{1}{2}\int_A \gamma^T D_s \gamma \, dxdy \tag{9}$$

and

$$D_b = \int_{-h/2}^{h/2} D(z) z^2 dz \tag{10}$$

$$D_s = k\int_{-h/2}^{h/2} E(z)\, dz\, k \tag{11}$$

The variables U_b and U_s represent the bending and transverse shear contributions, respectively, and k in equation (11) contains shear correction factors to account for the non-uniformity of the transverse shear stresses through the plate thickness.

In equations (8) and (9) the matrices D_b and D_s are functions of the thickness of plate, h, and of the elastic properties of the different layers. The variable A is the area of the middle surface of the plate. For an isotropic homogeneous plate of constant thickness D_b and D_s become:

$$D_b = \frac{Eh^3}{12(1-\nu^2)}\begin{bmatrix} 1 & \nu & 0 \\ & 1 & 0 \\ & & \frac{1-\nu}{2} \end{bmatrix}$$

$$D_s = \frac{Ehk}{2(1+\nu)}\begin{bmatrix} 1 & 0 \\ 0 & 1 \end{bmatrix} \tag{12}$$

The explicit expressions U_b and U_s are then:

$$U_b = \frac{Eh^3}{24(1-\nu^2)}\int_A \left\{\beta_{x,x}^2 + \beta_{y,y}^2 + 2\nu\beta_{y,y}\beta_{x,x} + \frac{1-\nu}{2}(\beta_{y,x} + \beta_{x,y})^2\right\}dxdy \tag{13}$$

$$U_s = \frac{Ehk}{4(1+\nu)}\int_A \left\{(w_{,x} + \beta_x)^2 + (w_{,y} + \beta_y)^2\right\}dxdy \tag{14}$$

The variables E and ν in equations (12) and (14) are the Young's modulus and Poisson's ratio, respectively, and k is the shear correction factor usually taken as 5/6.

By definition, the bending moments **M** and shear forces **Q** are obtained by integration of the stresses through the element thickness, h:

$$\mathbf{M} = \begin{bmatrix} M_x \\ M_y \\ M_z \end{bmatrix} = \int_{h/2}^{h/2} \sigma z \, dz = \mathbf{D}_b \boldsymbol{\kappa} \tag{15}$$

and

$$\mathbf{Q} = \begin{bmatrix} Q_x \\ Q_y \end{bmatrix} = \mathbf{k}\int_{h/2}^{h/2} \sigma_s dz \mathbf{k} = \mathbf{D}_s \boldsymbol{\gamma} \tag{16}$$

The expression of U as given by equations (7) through (9), or (13) and (14), is used to formulate finite elements for the analysis of plates where the transverse shear effects are important. The independent quantities subjected to variation are w, β_x and β_y with the conditions on the part of the boundary where displacements are prescribed.

2.2 Stiffness matrix of the DKT element

The formulation of the DKT element as presented in References [7] through [10] is based on the assumption that β_x and β_y vary quadratically over the element, i.e.:

$$\begin{aligned} \beta_x &= \sum_{i=1}^{6} N_i \beta_{x_i} \\ \beta_y &= \sum_{i=1}^{6} N_i \beta_{y_i} \end{aligned} \tag{17}$$

where β_{x_i} and β_{y_i} are the nodal values at the corners, and at the mid-nodes, the $N_i(\xi,\eta)$ are the shape functions given in Appendix A, ξ and η are the coordinates.

Introducing the vector of the nodal degrees of freedom:

$$\mathbf{U}^T = [w_1\ \theta_{x_1}\ \theta_{y_1}\ w_2\ \theta_{x_2}\ \theta_{y_2}\ w_3\ \theta_{x_3}\ \theta_{y_3}\ w_4\ \theta_{x_4}\ \theta_{y_4}\ w_5\ \theta_{x_5}\ \theta_{y_5}\ w_6\ \theta_{x_6}\ \theta_{y_6}] \tag{18}$$

and using equations (17) and (18), the following expressions are obtained for β_x and β_y:

$$\begin{aligned} \beta_x &= \mathbf{H}_x^T(\xi,\eta)\mathbf{U} \\ \beta_y &= \mathbf{H}_y^T(\xi,\eta)\mathbf{U} \end{aligned} \tag{19}$$

where H_x and H_y are the nine component vectors of the shape functions. The components are functions of the N_i, i = 1, 6 and of the coordinates of the nodes:

$$
\begin{aligned}
H_{x_1} &= 1.5\ (a_6N_6 - a_5N_5) \\
H_{x_2} &= b_5N_5 + b_6N_6 \\
H_{x_3} &= N_1 - c_5N_5 - c_6N_6
\end{aligned}
$$

$$
\begin{aligned}
H_{x_4} &= 1.5\ (a_4N_4 - a_6N_6) \\
H_{x_5} &= b_4N_4 + b_6N_6 \\
H_{x_6} &= N_2 - c_4N_4 - c_6N_6
\end{aligned}
\qquad (20)
$$

$$
\begin{aligned}
H_{x_7} &= 1.5\ (a_5N_5 - a_4N_4) \\
H_{x_8} &= b_4N_4 + b_5N_5 \\
H_{x_9} &= N_3 - c_4N_4 - c_5N_5
\end{aligned}
$$

$$
\begin{aligned}
H_{y_1} &= 1.5\ (d_6N_6 - d_5N_5) \\
H_{y_2} &= -N_1 + e_5N_5 + e_6N_6 \\
H_{y_3} &= -H_{x_2}
\end{aligned}
$$

$$
\begin{aligned}
H_{y_4} &= 1.5\ (d_4N_4 - d_6N_6) \\
H_{y_5} &= -N_2 + e_4N_4 + e_6N_6 \\
H_{y_6} &= -H_{x_2}
\end{aligned}
\qquad (21)
$$

$$
\begin{aligned}
H_{y_7} &= 1.5\ (d_5N_5 - d_4N_4) \\
H_{y_8} &= -N_3 + e_4N_4 + e_5N_5 \\
H_{y_9} &= -H_{x_2}
\end{aligned}
$$

Also,

$$a_k = -\frac{x_{ij}}{(x_{ij}^2 + y_{ij}^2)}$$

$$b_k = \frac{3}{4}\frac{x_{ij}y_{ij}}{(x_{ij}^2 + y_{ij}^2)}$$

$$c_k = \frac{(0.25x_{ij}^2 - 0.5y_{ij}^2)}{(x_{ij}^2 + y_{ij}^2)} \qquad (22)$$

$$d_k = -\frac{y_{ij}}{(x_{ij}^2 + y_{ij}^2)}$$

$$e_k = \frac{(0.25y_{ij}^2 - 0.5x_{ij}^2)}{(x_{ij}^2 + y_{ij}^2)}$$

where $k = 4,5,6$ for the sides $ij = 23,\ 31,\ 12$ respectively.

The evaluation of the stiffness matrix follows the standard procedures of the finite element displacement method. Using equations (4) and (19),

$$\kappa = \mathbf{B}U \qquad (23)$$

where **B** is the strain-displacement transformation matrix given in Appendix A.

The stiffness matrix of the DKT element becomes

$$K_{DKT} = 2A\int_0^1 \int_0^{1-\eta} \mathbf{B}^T\mathbf{D}_b\mathbf{B}\, d\xi d\eta \qquad (24)$$

The bending moments **M** at any point in the element can be obtained using equations (15) and (23):

$$\mathbf{M}(x,y) = \mathbf{D}_b\mathbf{B}(x,y)\mathbf{U} \qquad (25)$$

where

$$x = x_1 + \xi x_{21} + \eta x_{31}$$
$$y = y_1 + \xi y_{21} + \eta y_{31} \quad (26)$$

Since, **M** depends upon all the components of **U**, **M** is not unique along the boundary shared by two elements.

The theoretical predictions presented in this study are obtained using a finite element mesh consisting of 6085 elements as shown in Figure 2.

3. PERFORMANCE OF THE HELICOPTER

In this section, the experimental performance of the helicopter is determined and compared with the theoretical predictions as obtained from the finite element models described in section 2.

3.1 Material Properties

A Ultrasport helicopter cabin (Model ATI-496) is considered, with a width of 2.438 m (8 feet) and height of 2.388 m (7ft. 10 inches) as shown in Figure 3. The helicopter cabin is made of a total of three different materials. The windows are made of acrylic with Young's modulus is 3E9 Pa and density is 1310 kg/m^3. The seat which is used for passenger compartment flooring and ribs are made of a honeycomb composite fiberglass, which is an aircraft grade sandwich panel made from high impact fiberglass epoxy facing bonded to a honeycomb core. The fiberglass Young's Modulus is 0.146E9

Pa and its density is 230 kg/m^3. The remaining parts of the helicopter cabin are made of a composite fiberglass whose Young's Modulus is 7.8E9 Pa and density is 1600 kg/m^3. The mechanical properties and geometrical parameters of the different materials in the helicopter cabin are summarized in Table 1. A photograph of the helicopter cabin and ribs is shown in Figures 3(a) and 3(b).

3.2 Experimental set-up

3.2.1 Helicopter Door measurement

The door is suspended to the ceiling of the laboratory using flexible hanging cables. The test door is acoustically excited by a speaker driven by the signal source of a FFT analyzer (Model CF910, ONO Sokki) through a power Amplifier (Model 6260, JBL. Urel Electronic Co.). The amplitude of vibration of the door is monitored by the scanning of its vibrating surface using a scanning laser vibrometer (Polytec PI PSV-300, Auburn, MA). It is important here to note that the test door is checked in order to accurately predict its mode shapes and therefore study the helicopter cabin perfectly.

3.2.2 Helicopter cabin measurement

The tests carried out on the helicopter cabin experiment are conducted in an anechoic chamber. A photograph of the helicopter cabin and the anechoic chamber is shown in Figure 3. The test cabin is excited by a white noise excitation through a shaker

mounted back wall of the cabin. The amplitude of vibration of the helicopter cabin is monitored using a scanning laser vibrometer (Polytec PI PSV-300, Auburn, MA).

3.3 Numerical and Experimental Results

The finite element model for the door is first verified. The natural frequencies of the free-free door obtained by this model are compared by those obtained experimentally and presented in Table 2. The numerical predictions are in good agreement with the experimental results. The first three mode shapes of the door are shown in Figure 4. Figure 4 shows the mode shapes corresponding to the frequencies listed in Table 2. In order to identify the mode shapes and the associated deflections, the surface of the door is scanned using a laser vibrometer for modes in free-free boundary condition, respectively. A comparison between the experimental and theoretical natural frequencies is presented in Figure 5. The figure clearly indicates the good agreement between theoretical predictions and the experimental results.

Next, the helicopter cabin inside anechoic chamber is chosen to measure the natural frequencies and mode shapes. The natural frequencies of the helicopter cabin are computed the FE model and are also determined experimentally as shown in Table 3. Figure 6 display the mode shapes of the FE model corresponding to the frequencies shown in Table3. Figure 7 shows a comparison between the theoretical predictions and experimental results.

5 CONCLUSIONS

This paper has presented the finite element modeling of the helicopter cabin and its door. The model is developed to predict the frequencies and mode shapes from such a commercial helicopter. The predictions of the finite element model are validated by comparing the predicted dynamic characteristics, such as natural frequencies and mode shapes, with those obtained experimentally. Excellent agreement is obtained between the predictions of the finite element and the experimental results.

A natural extension of the present study is to augment the passive control of vibration and noise radiation from helicopter cabin using Passive Constrained Layer Damping (PCLD) treatment placed in strategical locations in the cabin and its door. Additional work is needed to study theoretically and experimentally the flow of the vibrational energy through the entire cabin of the helicopter in an attempt to control the transmission paths from the excitation zones to the critical locations along the helicopter.

ACKNOWLEDGMENTS

This work has been funded by the Army Research Office (ARO) (Grants Number DAAH-04-96-1-0317 and DAAG-55-98-1-0206). Special thanks are due to Dr. Gary Anderson, the technical monitor from ARO, for his invaluable inputs.

APPENDIX

A.1 Shape functions for DKT element

$$
\begin{aligned}
N_1 &= 2(1-\xi-\eta)(\frac{1}{2}-\xi-\eta) \\
N_2 &= \xi(2\xi-1) \\
N_3 &= \eta(2\eta-1) \\
N_4 &= 4\xi\eta \\
N_5 &= 4\eta(1-\xi-\eta) \\
N_6 &= 4\xi(1-\xi-\eta)
\end{aligned}
\tag{A.1}
$$

ξ and η are the area coordinates L_2 and L_3 [11].

A.2 Strain-displacement transformation matrix

The matrix of strain-displacement is given by:

$$
B(\xi,\eta) = \frac{1}{2A}\begin{bmatrix} y_{31}H^T_{x,\xi} + y_{12}H^T_{x,\eta} \\ -x_{31}H^T_{y,\xi} - x_{12}H^T_{y,\eta} \\ -x_{31}H^T_{x,\xi} - x_{12}H^T_{x,\eta} + y_{31}H^T_{y,\xi} + y_{12}H^T_{y,\eta} \end{bmatrix} \tag{A.2}
$$

where $2A = x_{31}y_{12} - x_{12}y_{31}$.

REFERENCES

[1] Unruh, J. F., "Procedure for Evaluation of Engine Isolators for Reduced Structure-Borne Noise Transmission", J. of Aircraft, Vol. 20, NO. 1, Jan. (1983) 76-82.

[2] Unruh, J. F. and Fox, D. J., "A study of Rotorcraft Structure-Borne Nois Isolation Using Empirical Component Coupling", J. of the American Helicopter society, July (1999) 172-178.

[3] Swanson, D. A., Miller, L. R. and Norris, M. A., "Multidimensional Mount Effectiveness for Vibration Isolation", J. of Aircraft, Vol. 31, NO. 1, Jan.-Feb. (1994) 188-196.

[4] Sutton, T. J., Elliott S. J., Brennan, M. J. Heron, K. H. and Jessop, D. A. C., "Active Isolation of Multiple Structural Waves on a Helicopter Gearbox support Strut", J. of Sound and Vibration, 205(1) (1997) 81-101.

[5] Bathe, K. J., *Finite Element Procedures in Engineering Analysis*, Prentice Hall, Englewood Cliffs, New York, 1996.

[6] Razzaque, A., "On the Four Noded Discrete Kirchhoff Shell Elements", Ribinson, J. (ed.), Accuracy Reliability Training in FEM Technology, (1984) 473-483.

[7] Stricklin, J. A., Haisler, W., Tisdale, P. and Gunderson, R., "A rapidly converging triangular plate element", AIAA J. **7** (1), (1969) 180-181.

[8] Dhatt, G., "Numerical analysis of thin shells by curved triangular elements based on discrete Kirchhoff hypothesis", Proc. ASCE Symp. On Applications of FEM in Civil Engineering, Vanderbilt Univ., Nashville, Tenn., (1969) 13-14.

[9] Dhatt, G., "An efficient triangular shell element", AIAA J. **8** (11), (1970) 2100-2102.

[10] Dhatt, G. and Venkatasubbu, S., "Finite element analysis of containment vessels", Proc. First Conf. On Struct. Mech. In Reactor Tech., vol. 5, Berlin, Germany, 1971.

[11] Zienkiewicz, O. C., Finite element Method, 3rd Ed. McGraw-Hill, London, 1977.

NOMENCLATURE

x, y, z	Cartesian coordinates;
u, v, w	displacements;
β_x, β_y	Rotation of the middle surface;
η	loss factor of viscoelastic;
ε_b	bending strain;
γ	transverse strain;
κ	component vector of curvature;
τ	Shear stress;
σ_b	bending stress vector;
σ_s	shear stress vector;
B	transformation matrix;
D	constitutive matrix;
K_{DKT}	stiffness matrix;
N	matrix of shape functions;
$E_{i,j}$	The component of the three-dimensional elasticity matrix;
E	Young's modulus;
U_b	strain energy of bending;
U_s	strain energy of shear;
U	strain energy;
h	thickness of layer;

M bending moment;

Q Shear force;

T kinetic energy;

TABLES

Table 1: Properties of the Helicopter Cabin

	Young's Modulus [Pa]	Density [kg/m^3]	Thickness [m]
Window	5.0E9	1310	1.4E-3
Skin	12E9	1650	1.4E-3
Back, Seat & Ribs	0.146E9	230	10.16E-3
Skid	0.4E9	2700	*

Table 2: Natural frequencies [Hz] of different door configurations.

Mode	Experiment	FEM
1	10.3	10.25
2	12.5	12.94
3	21.2	25.46

Table 3: Natural frequencies [Hz] of different helicopter cabin configurations.

Mode Shapes	Theoretical	Experimental
Bottom 1st Bending	7.57	7
Bottom 2nd Bending	14.86	13.5
Door (Window) & Bottom Torsion	17.16	15.5
Door	22.43	26.5
Front Window	62.61	65

LIST OF FIGURES

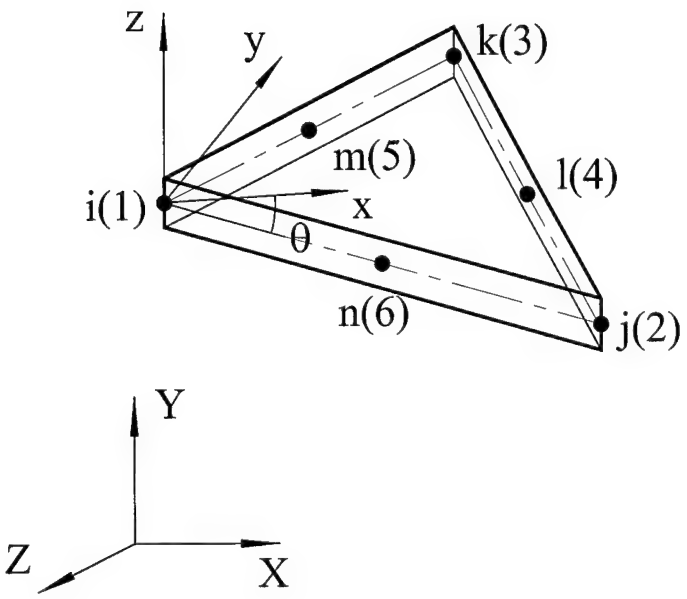

Figure 1: The coordinate system for the structural shell element

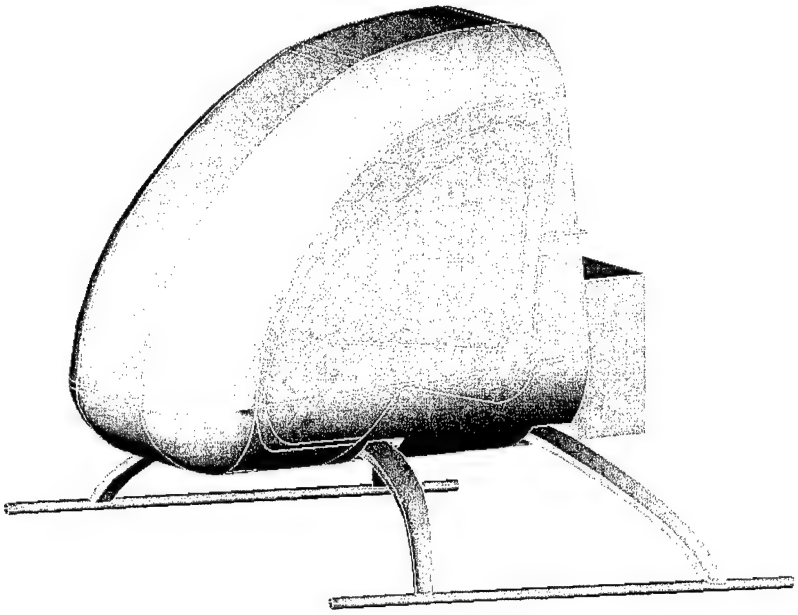

(a)

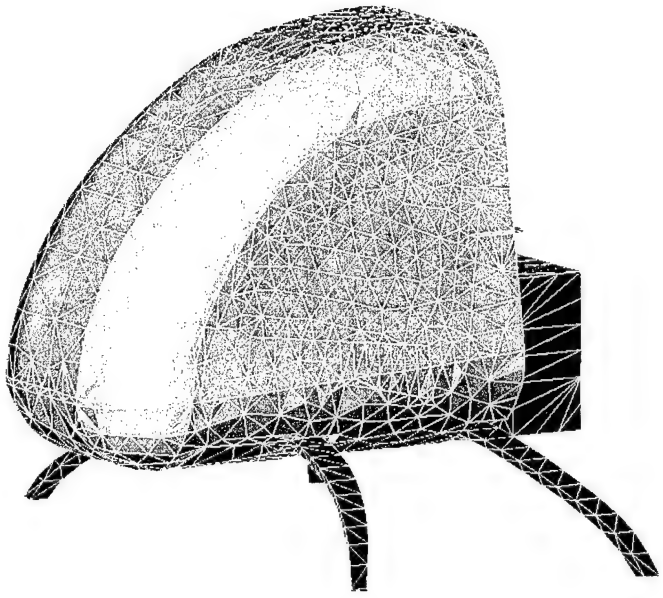

(b)

Figure 2: Finite Element model of the Test Article: Solid Model (a), and FEM (b)

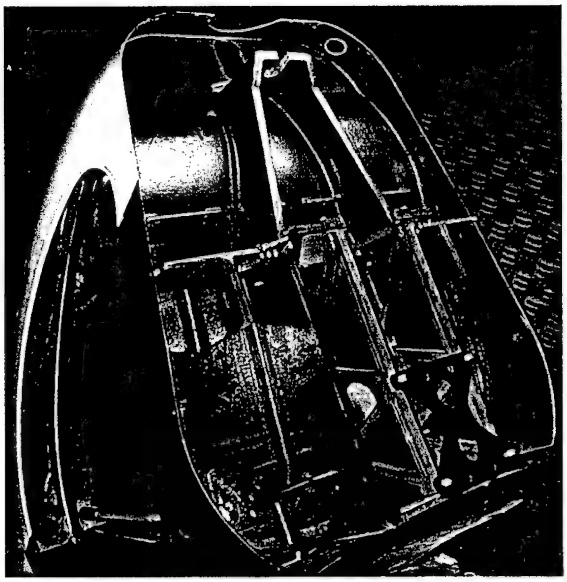

(a)

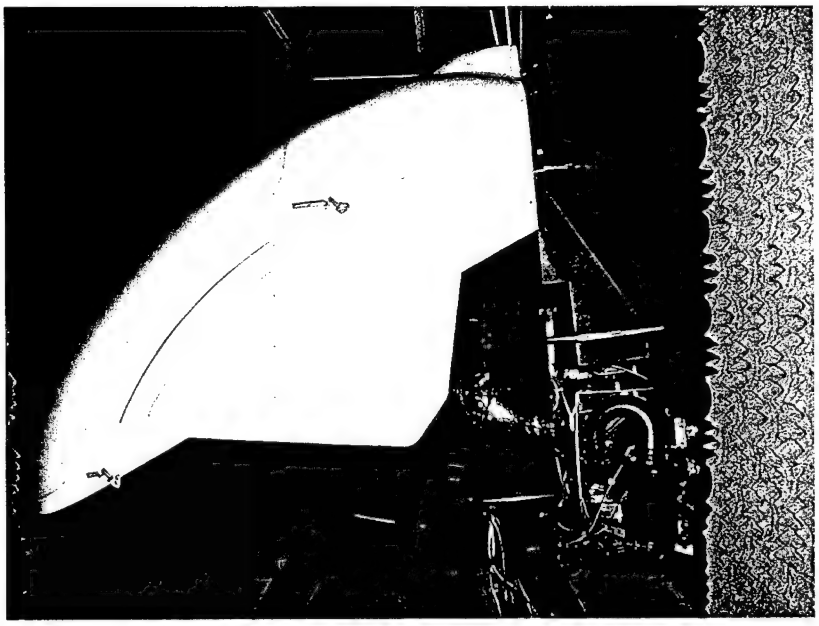

(b)

Figure 3: Photographs of the experimental helicopter and setup

1st Mode

(a)

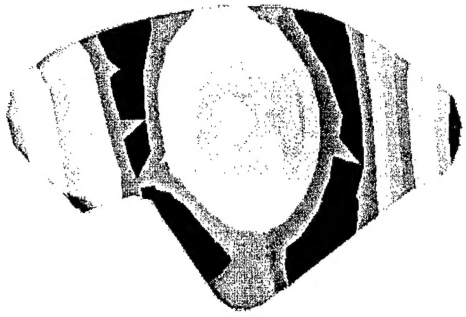

(b)

2nd Mode

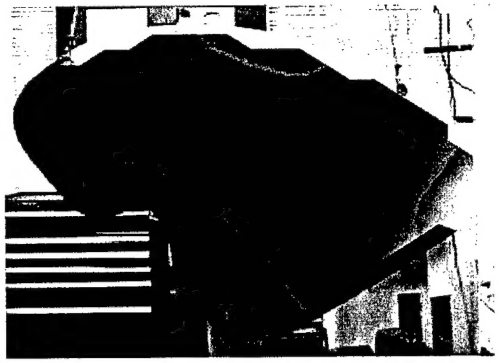

(a)

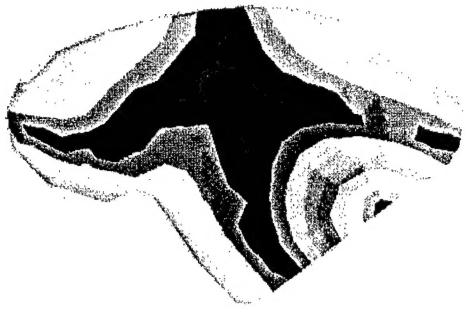

(b)

3rd Mode

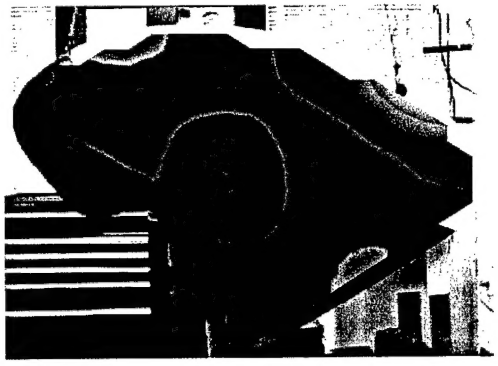

(a)

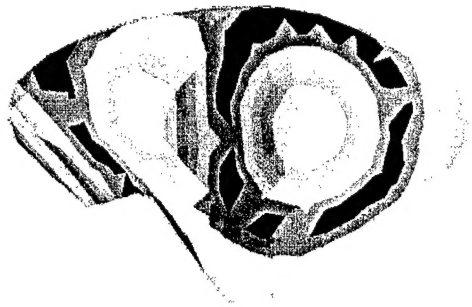

(b)

Figure 4: Modes of the Helicopter Door:
(a) Experiment, (b) FEM

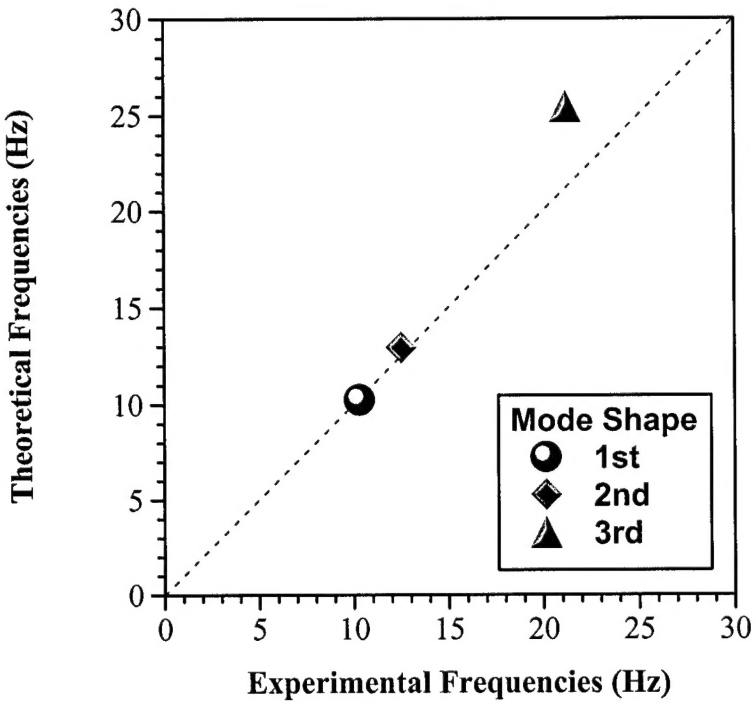

Figure 5: Comparison between Experimental and Theoretical Natural Frequencies of the Helicopter Door

1st Mode of Bottom (7.57 Hz)

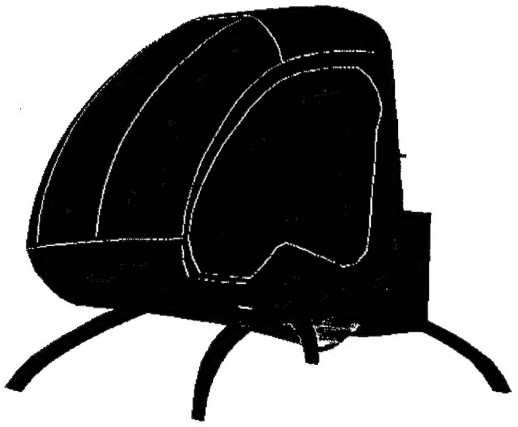

2nd Mode of Bottom (14.86 Hz)

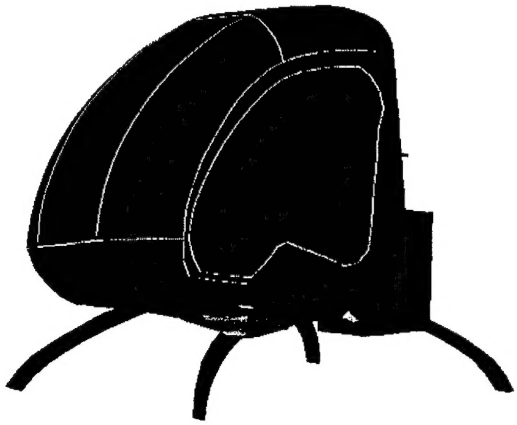

1st Mode of Door (16.59 Hz)

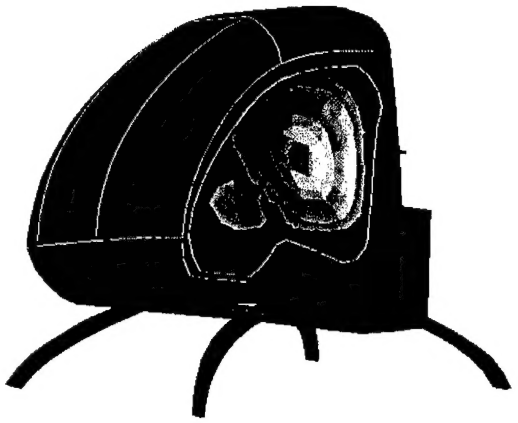

1st Mode of Front Shield (62.61 Hz)

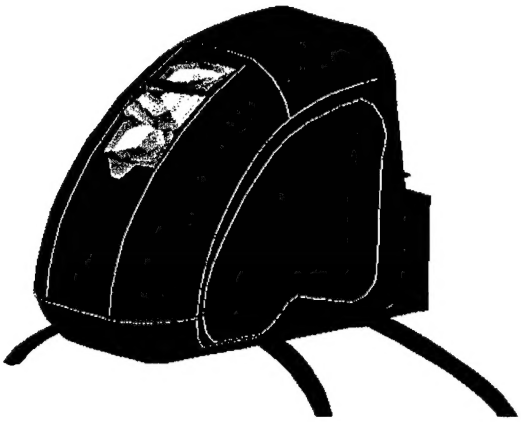

Figure 6: Modes of the Helicopter Cabin using FEM:

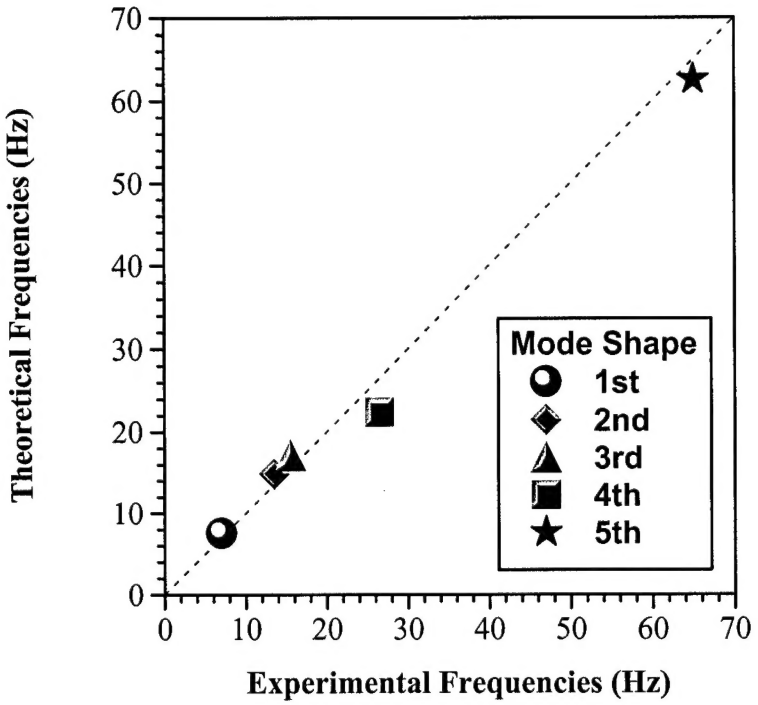

Figure 7: Comparison between Experimental and Theoretical Natural Frequencies of the Helicopter Cabin